Croatian Society for Materials Protection

Metalurgija/Metallurgy

Vol. 65 No. 4 / 2026

Microstructural Evolution of the Hot Rolling Interface in 304 Stainless Steel/Q235 Carbon Steel Clad Plates for Microphone Pop Filters

Bin Sun

https://doi.org/10.64486/m.65.4.4

School of Music and Dance, Harbin University, China; 15104629776@163.com

Type of the Paper: *Article*
Received: December 12, 2025
Accepted: February 26, 2026

Abstract: In response to the comprehensive requirements of microphone pop filters for materials' corrosion resistance and structural stability, 304 stainless steel/Q235 carbon steel clad plates have emerged as the preferred choice due to their superior performance and the hot rolling process is crucial to ensuring the bonding quality of the interface. Taking this clad plate as the research object, this study systematically investigates the influence laws of the hot rolling process on the evolution of interface microstructure and bonding characteristics by comparing annealed samples with double hot-rolled ones. The results indicate that a sound metallurgical bond is formed between the 304 layer and the Q235 layer, with the microstructures on both sides of the interface being austenite and ferrite + pearlite, respectively; a ferrite decarburized layer with a thickness of approximately 140 μm forms on the Q235 side. After double hot rolling, the grains of the clad plate are significantly refined.

Keywords: hot rolling process; 304 stainless steel; Q235 carbon steel; interface microstructure; microphone pop filter

1. Introduction

With the development of microphone pop filters for audio equipment toward higher precision and greater reliability, stringent requirements have been imposed on material performance [1]. Materials used for microphone pop filters must combine the excellent corrosion resistance of stainless steel with the mechanical strength and formability of carbon steel to ensure structural stability in service environments [2]. The 304 stainless steel/Q235 carbon steel clad plate, with its balanced advantages of strong corrosion resistance, excellent mechanical properties, and low cost, has emerged as an ideal material for manufacturing microphone pop filters [3]. The bonding quality of its interface directly determines the overall service life of the clad plate [4]. As the core technology for the large-scale production of clad plates, the hot rolling process has gradually replaced explosive welding as the mainstream preparation method, owing to its high efficiency, good environmental compatibility, and reliable bonding performance [5].

Stainless steel/carbon steel clad plates integrate the excellent corrosion resistance and surface finish of stainless steel with the high mechanical strength, superior formability, and lightweight potential of carbon steel. Their interface behavior is a crucial determinant of material performance. However, most existing studies focus on general industrial applications, and few targeted studies have been conducted on the correlations between process, interface microstructure and properties for special scenarios with specific performance requirements [6]. Such scenarios impose more stringent requirements on the bonding compactness and grain size uniformity

of clad plate interfaces; interface defects or inhomogeneous microstructures tend to lead to structural failure. Nevertheless, the existing parameter system for the hot rolling process cannot be directly adapted to the customized requirements of these specific scenarios [7].

Based on this, this study takes the 304 stainless steel/Q235 carbon steel clad plate as the research object. By employing characterization techniques including Optical Microscopy (OM), Scanning Electron Microscopy (SEM), X-Ray Diffraction (XRD), and Electron Backscatter Diffraction (EBSD), this study systematically investigates the influence laws of the hot rolling process on the interface microstructure morphology, element diffusion characteristics, grain refinement and recrystallization behavior of the clad plates [8]. This study aims to provide a theoretical foundation and technical support for the precise preparation and performance optimization of such clad plates.

2. Experimental Materials and Methods

2.1 Composite Panel Preparation

Figure 1 shows the schematic of the preparation process for the experimental clad plates. The thicknesses of 304 stainless steel and Q235 carbon steel plates before rolling were 5 mm and 25 mm, respectively, and the total thickness of the 304 stainless steel/Q235 carbon steel composite billets was 30 mm. After hot rolling, the final thickness of the clad plates was 2 mm, with the 304 stainless steel layer being 0.5 mm thick and the Q235 carbon steel layer 1.5 mm thick. The chemical compositions of the clad plate are listed in Table 1.

Firstly, surface treatment was conducted on the Q235 carbon steel and 304 stainless steel plates separately: their surfaces were ground with sandpaper to remove oxide scale, exposing fresh metal substrates; subsequently, anhydrous ethanol was used to remove oil contaminants from the surfaces. The two plates were then stacked in the sequence of 304 stainless steel/Q235 carbon steel to form composite billets. After welding and vacuum sealing, the 30 mm-thick composite billets were heated to 1200 °C and held for 1 h in an RX_3-40-13 box-type resistance furnace, followed by hot rolling to a thickness of 10 mm (a total reduction ratio of 66.67 %). The rolled plates were air-cooled, then annealed at 500 °C for 1 h in the same RX_3-40-13 furnace and subsequently furnace-cooled; these samples were designated as annealed clad plates. The 10 mm-thick annealed plates were reheated to 800 °C and held for 10 min in the RX_3-40-13 furnace, then hot-rolled to 2 mm in thickness via 5 passes on a 200 mm two-high reversing hot rolling mill, with a total reduction ratio of 80 %, followed by air cooling. Finally, stress relief annealing was performed on the 2 mm-thick hot-rolled plates at 200 °C for 2 h in an SX_2-2.5-12 box-type resistance furnace.

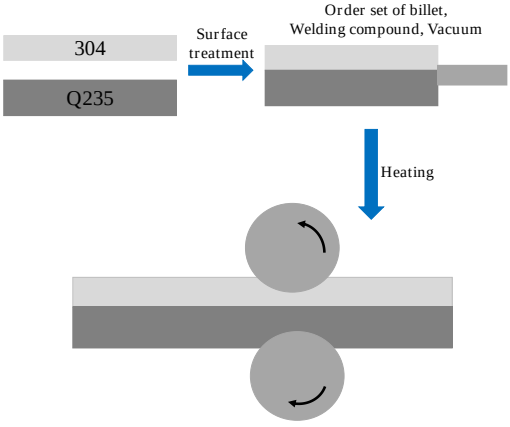

Figure 1. Schematic Diagram of Experimental Sample Preparation Process

Table 1. Chemical Compositions of 304 Stainless Steel/Q235 Carbon Steel Clad Plate (Mass Fraction, %)

Stell	C	Cr	Ni	Mn	Si	P	S	Fe
304	0.038	18.05	8.04	1.01	0.545	0.0645	0.021	Bal
Q235	0.25	0.0625	0.0356	1.07	0.365	0.0589	0.023	Bal

https://doi.org/10.64486/m.65.4.4

Samples were cut from the hot-rolled clad plates using a DK7745 wire electrical discharge machining (WEDM) machine. Firstly, the samples were ground with sandpapers of different grit sizes, then mechanically polished on a PG-2 polishing machine to obtain a mirror-finished surface. Subsequently, the polished surfaces were rinsed with anhydrous ethanol and dried with a hair dryer. Prior to microstructure observation and characterization, the stainless steel/carbon steel clad plate samples were subjected to chemical etching: the carbon steel side was etched with a 4% nitric acid-ethanol solution for 10–15 s, then rinsed with anhydrous ethanol and dried.

2.2 Microstructural Characterization

The microstructure of the clad plate was observed using a J-Y600 Optical Microscope (OM). A NANOSEM430 scanning electron microscope (SEM) equipped with an energy dispersive spectrometer (EDS) was employed to characterize the interfacial microstructures and elemental distribution. For Electron Backscatter Diffraction (EBSD) characterization, the samples were electrolytically polished in a perchloric acid-anhydrous ethanol solution (volume ratio 1:9) at 20 V for about 10 s to eliminate the surface stress layer. The surface of the hot-rolled clad plate samples was scanned using the same NANOSEM430 SEM equipped with an Oxford HKICHANNEL5 EBSD analysis system, with a scanning step size of 1 μm. Orientation Imaging Microscopy (OIM) maps were reconstructed via software analysis, from which grain boundary types and grain orientations were obtained.

Phase composition analysis was conducted on the annealed and hot-rolled 304 stainless steel/Q235 carbon steel clad plate samples using a Bruker D8 Advance X-ray diffractometer (XRD). During the tests, Co-Kα radiation was adopted for scanning over a 2θ range of 40°-120° at a scanning rate of 10°/min, with the electron gun operating at an acceleration voltage of 40 kV and a current of 40 mA. The obtained data were analyzed using Jade 6.0 software in combination with standard PDF cards.

2.3 Damping Performance Test

The damping properties of the samples were characterized using a TA Q800 Dynamic Mechanical Analyzer (DMA). Sample preparation: Strip samples with dimensions of 3 mm (width) × 20 mm (length) × 2 mm (thickness) were cut from the annealed and double hot-rolled composite plates, with the sample surfaces required to be flat and free of cracks.

Test parameters: A three-point bending mode was adopted, with the test temperature ranging from 25 °C to 200 °C (starting from room temperature), a heating rate of 5 °C/min, a frequency range of 20 Hz to 200 Hz, and an oscillation amplitude of 20 μm.

Characterization indices: The damping coefficient (tanδ) of the samples was recorded at different temperatures (25 °C, 40 °C, 60 °C, 80 °C, 100 °C) and frequencies (20 Hz, 40 Hz, 60 Hz, 80 Hz, 120 Hz, 160 Hz, 200 Hz). The damping coefficients at room temperature (25 °C) and 20 Hz, as well as at the peak frequency of plosive noise (40 Hz), were selected as the key evaluation indices.

3. Results and Discussion

To gain a detailed understanding of the microstructural evolution of hot-rolled 304 stainless steel/Q235 carbon steel clad plates, X-ray diffraction (XRD) was used to analyze their phase compositions, the results of which are shown in Figure 2. The XRD results show that diffraction peaks of γ-Fe and α-Fe are observed at 2θ = 51.1° and 59.7° for the annealed samples, and at 2θ = 52.3°, 77.1° and 99.5° for the double hot-rolled samples; γ-Fe and α-Fe correspond to the 304 stainless steel layer and Q235 carbon steel layer, respectively. Additionally, diffraction peaks of $Cr_{23}C_6$ are observed at 2θ = 59.7° and 99.5° for both sets of samples. Compared with the annealed state, the diffraction intensity of $Cr_{23}C_6$ in the double hot-rolled sample is reduced, and the diffraction peaks of γ-Fe and α-Fe exhibit significant broadening [9]. This phenomenon is attributed to the certain degree of grain refinement induced by the double hot rolling process.

https://doi.org/10.64486/m.65.4.4

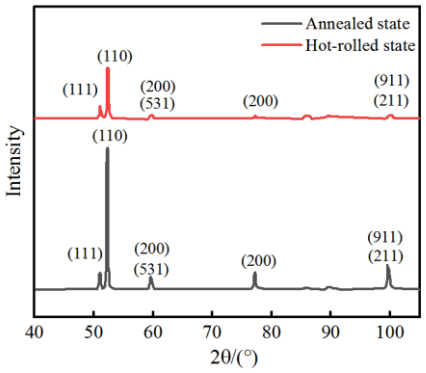

Figure 2. X-Ray Diffraction (XRD) Patterns of 304 Stainless Steel/Q235 Carbon Steel Clad Plates

Figure 3 shows the microstructure of the carbon steel side of the hot-rolled 304 stainless steel/Q235 carbon steel clad plate. As shown in Figure 3(a), the interface between the 304 layer and Q235 layer forms an excellent bond with no cracks or other defects, leading to strong interfacial adhesion of the clad plates [10]. No obvious defects such as pores are observed in the microstructure [11]. A distinct banded structure is formed on the carbon steel matrix side of the clad plates, which is attributed to an inappropriate rolling temperature. During hot rolling, when the rolling temperature is between A_{r1} and A_{r3}, ferrite precipitates in a banded manner along the rolling direction within the austenite matrix, while the remaining untransformed austenite is divided into bands. As the rolling temperature cools to A_{r1}, the banded austenite transforms into banded pearlite [12]. The Q235 layer is on the interfacial side of the clad plates, with its microstructure composed of ferrite and pearlite.

As shown in Figure 3(b), the carbon content of the carbon steel matrix is significantly higher than that of the stainless steel layer, leading to a higher carbon potential of the matrix during hot rolling and thus forming a large carbon concentration gradient between the cladding layer and the matrix [13]. Consequently, carbon atoms diffuse from the carbon steel side to the stainless steel side, causing decarburization on the carbon steel side and the formation of a 140 μm-thick decarburized layer with a fully ferritic microstructure.

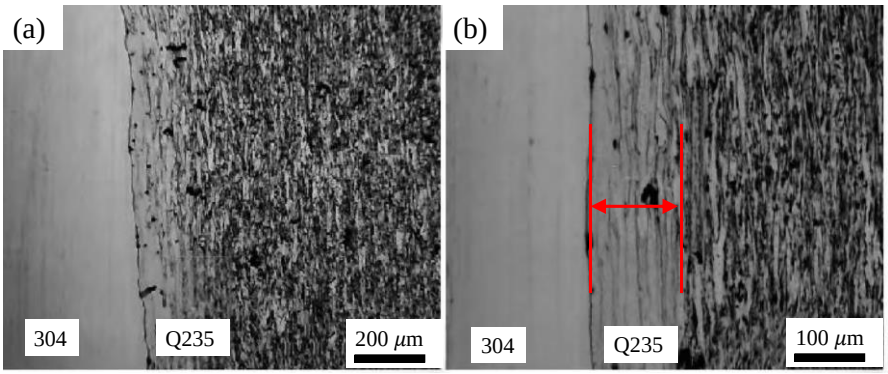

(a) microstructure of matrix carbon steel; (b) microstructure near the carbon steel side at the interface

Figure 3. Microstructure of carbon steel side of the 304 stainless steel/Q235 carbon steel hot rolled composite plate

Figure 4 presents the inverse pole figures (IPFs) and grain boundary maps of the annealed and hot-rolled 304 stainless steel/Q235 carbon steel clad plates. As observed in Figure 4(a), the grain color distribution of the annealed sample is relatively uniform, indicating a random grain orientation [14]. As shown in Figures 4(b) and 4(d), the content of high-angle grain boundaries (HAGBs) in the double hot-rolled samples is significantly lower than that in the annealed samples [15]. Grain size statistics were obtained using the linear intercept method, which shows that the average grain size of the annealed samples is about 22.45 μm on the carbon steel side and 16.84 μm on the stainless steel side, while the corresponding values for the double hot-rolled samples are 9.96 μm and 7.63 μm, respectively.

As shown in Figure 4(b), the interior of grains in the annealed sample is dominated by high-angle grain boundaries. In contrast to the annealed sample, Figures 4(c) and 4(d) illustrate a significant reduction in the

https://doi.org/10.64486/m.65.4.4

HAGB content within the grains of the hot-rolled sample. This decrease in HAGB content is attributed to a significant increase in the intragranular dislocation density during hot rolling, which causes an increase in the content of low-angle grain boundaries (LAGBs) and thus a corresponding decrease in HAGB content [16]. From the above analysis, it can be concluded that compared with the annealed state, the grains of the sample are significantly refined after double hot rolling [17].

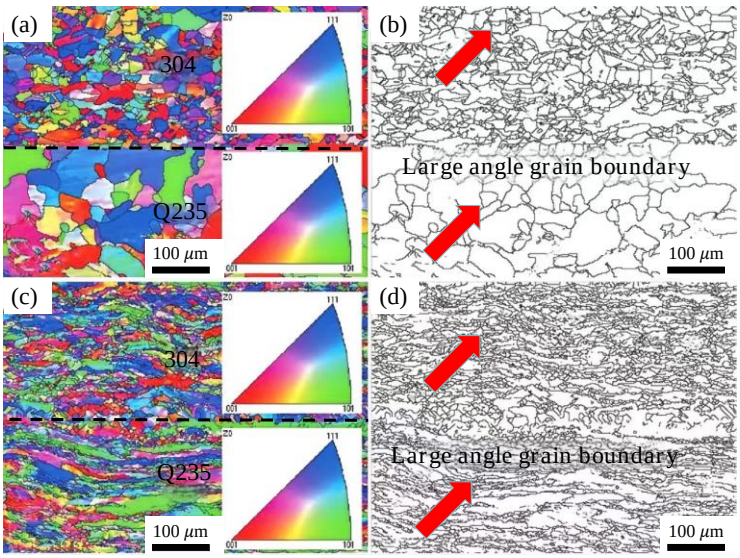

Figure 4. (a, c) Inverse Pole Figures (IPFs) and (b, d) Grain Boundary Maps of 304 Stainless Steel/Q235 Carbon Steel Clad Plates(a, b) Annealed State; (c, d) Hot-Rolled State

Figure 5 shows the recrystallization distribution maps of the annealed and double hot-rolled 304 stainless steel/Q235 carbon steel clad plates, and Figure 6 shows the volume fractions of different grain types in the clad plates under these two states. In Figure 5, blue grains represent recrystallized grains, yellow grains denote substructures (dislocations and subgrain boundaries), and red grains indicate deformed grains.

As observed in Figure 5(a) and Figure 6, both the 304 layer and Q235 layer of the annealed sample are dominated by deformed grains, with the volume fractions of deformed grains being 49.4 % and 64.9 %, respectively [18]. Compared with the annealed samples, the double hot-rolled samples show a significant decrease in the content of recrystallized and substructured grains, but a substantial increase in that of deformed grains [19].

From Figure 5(b) and Figure 6, for the hot-rolled sample, the volume fractions of deformed grains in the 304 layer and Q235 layer increased from 49.2 % and 62.5 % to 95.8 % and 97.0 %, respectively. Meanwhile, the volume fractions of recrystallized grains decreased from 21.2 % and 4.2 % to 2.9 % and 1.85 %, and those of substructure grains dropped from 31.8 % and 35.6 % to 1.5 % and 1.4 %, respectively.

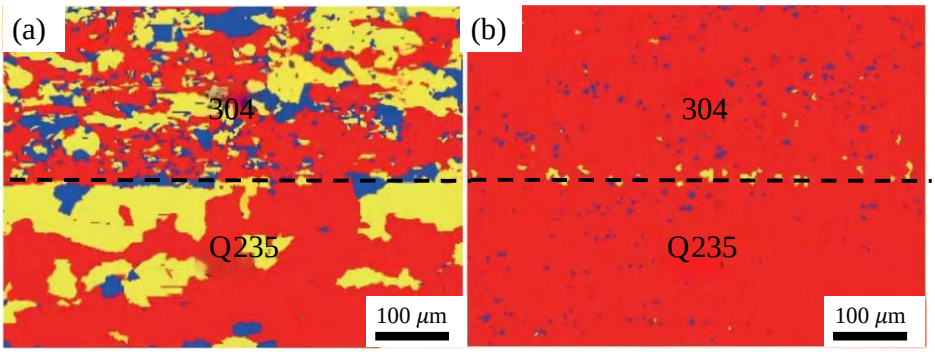

Figure 5. Recrystallization Distribution Maps of 304 Stainless Steel/Q235 Carbon Steel Clad Plates(a) Annealed State; (b) Hot-Rolled State

https://doi.org/10.64486/m.65.4.4

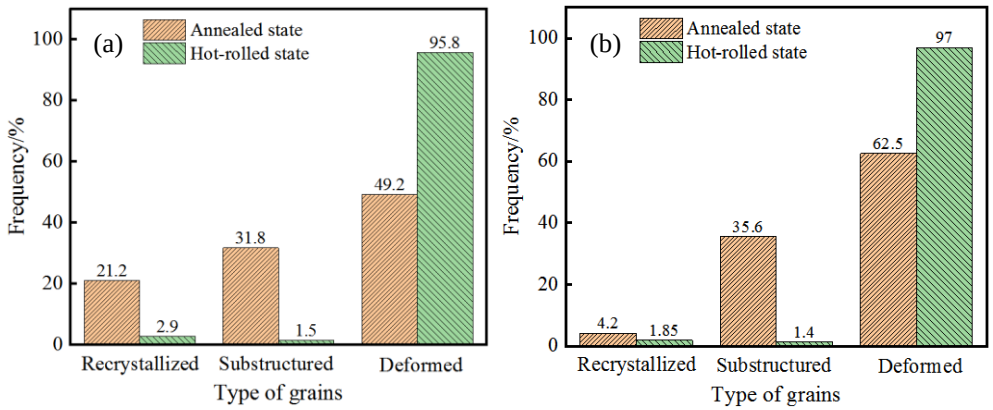

Figure 6. Specific Volume Fractions of Different Grain Types in Annealed and Hot-Rolled 304 Stainless Steel/Q235 Carbon Steel Clad Plates(a) 304 Layer; (b) Q235 Layer

Figure 7 shows the damping coefficient (tanδ) vs. temperature curves of the annealed and double hot-rolled composite plates at a frequency of 1 Hz. As shown in the figure, the damping coefficients of both plate states exhibit a trend of first stabilizing and then increasing with rising temperature [20]. Within the temperature range from 25°C to 200°C, the damping coefficient changes gradually.

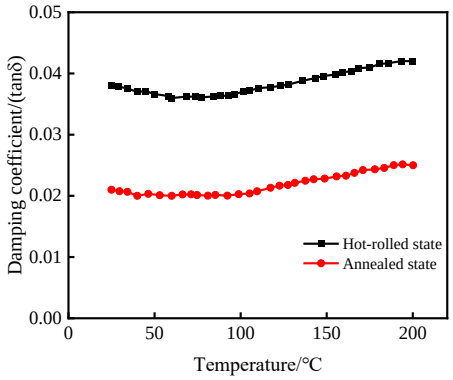

Figure 7. Temperature-Damping Coefficient Curves of Annealed and Hot-Rolled 304 Stainless Steel/Q235 Carbon Steel Clad Plates

Within the operational temperature range of microphone pop filter (25 °C–60 °C), the damping coefficient of double-pass hot-rolled composite plates maintains high stability: tanδ = 0.038 at 25 °C, tanδ = 0.037 at 40 °C, and tanδ = 0.036 at 60 °C, with a fluctuation range of only 5.3 %. In contrast, the annealed samples exhibit damping coefficients of 0.021 (25 °C), 0.020 (40 °C), and 0.020 (60 °C) within this temperature range, with a fluctuation range of 5 %. At temperatures exceeding 100 °C (extreme operating conditions), the tanδ of the double-pass hot-rolled sample increased to 0.042, yet remained significantly higher than that of the annealed sample (0.025), demonstrating its excellent damping stability across a wide temperature range [21].

Figure 8 shows the damping coefficient variation curves of annealed and double-pass hot-rolled composite plates in the 20 Hz-200 Hz frequency range at room temperature (25 °C). The figure indicates that the damping coefficients of both plate states decrease with increasing frequency, but exhibit distinct trends [22]. The tanδ of the hot-rolled samples remains between 0.033 and 0.038, with values of tanδ = 0.037 at 40 Hz and tanδ = 0.036 at 80 Hz. In contrast, the tanδ of the annealed samples in the corresponding frequency range is only 0.018-0.021, with tanδ = 0.020 at 40 Hz and tanδ = 0.019 at 80 Hz.

https://doi.org/10.64486/m.65.4.4

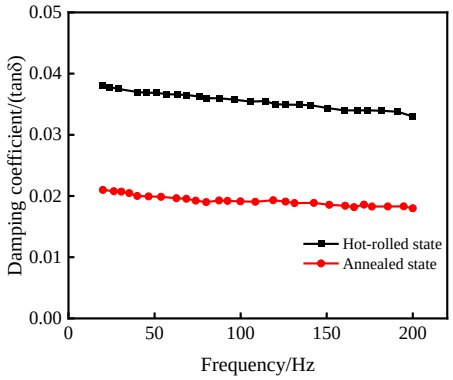

Figure 8. Frequency-Damping Coefficient Curves of Annealed and Hot-Rolled 304 Stainless Steel/Q235 Carbon Steel Clad Plates

4. Conclusions

The microstructure at the interface of hot-rolled 304 stainless steel/Q235 carbon steel composite plates is as follows: the 304 layer exhibits an austenitic structure, while the Q235 layer consists of a ferritic + pearlitic structure. A decarburized ferrite layer approximately 140 μm thick exists within the Q235 layer. This decarburized layer further enhances the material's toughness, preventing brittle fracture of the microphone pop filter due to impacts during handling and service, while also establishing the structural foundation for improved damping performance.

Following double-pass hot rolling, grain refinement is significantly enhanced: grain size in the stainless steel layer decreases from 16.84 μm to 7.63 μm, while grain size in the carbon steel layer reduces from 22.45 μm to 9.96 μm. The synergistic optimization of microstructure (target phase composition, ferrite decarburization layer, and grain refinement) substantially enhances the material's damping properties. At 25 °C and 40 Hz (the peak frequency of plosive noise), the damping coefficient (tanδ) reaches 0.037, effectively dissipating vibration energy induced by plosive noise and reducing residual low-frequency noise. This enables the composite plate to achieve "lightweight and thin-walled" characteristics while maintaining high strength and excellent vibration damping. When applied to microphone pop filters, it allows for the production of thinner, lighter pop filter products without compromising structural strength or acoustic performance. Additionally, the lightweight design is better suited for portable applications such as handheld microphones and wireless microphones, enhancing user convenience.

References

[1] E. K. Kokkinis, J. D. Reiss, and J. Mourjopoulos, "A Wiener filter approach to microphone leakage reduction in close-microphone applications," *IEEE Transactions on Audio, Speech, and Language Processing*, vol. 20, no. 3, pp. 767-779, 2012, https://doi.org/10.1109/TASL.2011.2164534

[2] S. Wang et al., "Microstructure, mechanical properties and interface bonding mechanism of hot-rolled stainless steel clad plates at different rolling reduction ratios," *Journal of Alloys and Compounds*, vol. 766, pp. 517-526, 2018, https://doi.org/10.1016/j.jallcom.2018.06.109

[3] Yi, Yali, et al. "Analysis of microstructure and properties evolution of asynchronous hot rolled stainless steel clad plate with interlayer." *Materials Today Communications*, vol. 42, pp. 111380, 2025, https://doi.org/10.1016/j.mtcomm.2024.111380

[4] M. S. Sihabbudin, F. Chandra, and S. A, "Characteristics of hot rolled stainless steel-clad plate with and without interlayer: a review," *Metallurgical Research & Technology*, vol. 122, no. 4, pp. 406, 2025, https://doi.org/10.1051/metal/2025033

[5] B. X. Liu et al., "Meso and microscale clad interface characteristics of hot-rolled stainless steel clad plate," *Materials Characterization*, vol. 148, pp. 17-25, 2019, https://doi.org/10.1016/j.matchar.2018.12.008

https://doi.org/10.64486/m.65.4.4

[6] Z. Zhu et al., "Effect of interface oxides on shear properties of hot-rolled stainless steel clad plate," *Materials Science and Engineering A*, vol. 669, pp. 344-349, 2016, https://doi.org/10.1016/j.msea.2016.05.066

[7] B. X. Liu et al., "Interface formation and bonding mechanisms of hot-rolled stainless steel clad plate," *Journal of Materials Science*, vol. 54, no. 17, pp. 11357-11377, 2019, https://doi.org/10.1007/s10853-019-03581-x

[8] B. X. Liu et al., "Microstructure and mechanical properties of hot rolled stainless steel clad plate by heat treatment," *Materials Chemistry and Physics*, vol. 216, pp. 460-467, 2018, https://doi.org/10.1016/j.matchemphys.2018.06.033

[9] B. X. Liu et al., "Interface characteristics and fracture behavior of hot rolled stainless steel clad plates with different vacuum degrees," *Applied Surface Science*, vol. 463, pp. 121-131, 2019, https://doi.org/10.1016/j.apsusc.2018.08.221

[10] J. Jiang et al., "Interfacial microstructure and mechanical properties of stainless steel clad plate prepared by vacuum hot rolling," *Journal of Iron and Steel Research International*, vol. 25, no. 7, pp. 732-738, 2018, https://doi.org/10.1007/s42243-018-0090-7/metrics

[11] S. Wang et al., "Microstructure and Interface Fracture Characteristics of Hot‐Rolled Stainless Steel Clad Plates by Adding Different Interlayers," *Steel Research International*, vol. 91, no. 4, pp. 1900604, 2020, https://doi.org/10.1002/srin.201900604

[12] J. Chen et al., "Interfacial Microstructure and Cladding Corrosion Resistance of Stainless Steel/Carbon Steel Clad Plates at Different Rolling Reduction Ratios," *Metals*, vol. 15, no. 1, pp. 16, 2024, https://doi.org/10.3390/met15010016

[13] Y. Yang et al., "Effect of Hot Rolling Temperature on Microstructure and Mechanical Properties of Horizontal Continuous Liquid-Solid Composite Cast Stainless Steel Clad Plate," *Steel Research International*, vol. 97, pp. 395-404, 2025, https://doi.org/10.1002/srin.202500111

[14] Y. Liu et al., "Deformation mechanism and microstructure evolution in stainless steel clad plate of longitudinal corrugated hot rolling," *Journal of Materials Processing Technology*, vol. 316, pp. 117957, 2023, https://doi.org/10.1016/j.jmatprotec.2023.117957

[15] Z. Zhao et al. "Effect of rolling temperature on microstructure and mechanical properties of Ti/steel clad plates fabricated by cold spraying and hot-rolling," *Materials Science and Engineering: A*, vol. 795, pp. 139982, 2020, https://doi.org/10.1016/j.msea.2020.139982

[16] G. Xie et al., "Interface characteristic and properties of stainless steel/HSLA steel clad plate by vacuum rolling cladding," *Materials Transactions*, vol. 52, no. 8, pp. 1709-1712, 2011, https://doi.org/10.2320/matertrans.M2011127

[17] J.-C. Jin et al., "Microstructures and intergranular corrosion resistances of hot-rolled austenitic stainless steel clad plates," *Journal of Materials Research and Technology*, vol. 26, pp. 1-13, 2023, https://doi.org/10.1016/j.jmrt.2023.07.192

[18] C. Yu et al., "Effect of pure iron interlayer on microstructure and properties of hot-rolled stainless steel clad plate," *Materials Today Communications*, vol. 28, pp. 102497, 2021, https://doi.org/10.1016/j.mtcomm.2021.102497

[19] Z. Dhib et al., "Cladding of low-carbon steel to austenitic stainless steel by hot-roll bonding: microstructure and mechanical properties before and after welding," *Materials Science and Engineering: A*, vol. 656, pp. 130-141, 2016, https://doi.org/10.1016/j.msea.2015.12.088

[20] Schaller, R. "Metal matrix composites, a smart choice for high damping materials." *Journal of Alloys and Compounds*, vol. 355, no. 1-2, pp. 131-135, 2003, https://doi.org/10.1016/s0925-8388(03)00239-1

[21] Adams, R. D. "The damping characteristics of certain steels, cast irons and other metals." *Journal of Sound and Vibration*, vol. 23, no. 2, pp. 199-216, 1972, https://doi.org/10.1016/0022-460x(72)90560-3

[22] Kappe, Konstantin, et al. "Design and manufacturing of a metal-based mechanical metamaterial with tunable damping properties." *Materials*, vol. 15, no. 16, pp. 5644, 2022, https://doi.org/10.3390/ma15165644